Two-dimensional surrogate Hamiltonian investigation of laser-induced desorption of NO/NiO(100)

Sören Dittrich[a] and Hans-Joachim Freund
Fritz-Haber-Institut der Max-Planck-Gesellschaft, Faradayweg 4-6, D-14195 Berlin, Germany

Christiane P. Koch and Ronnie Kosloff
Department of Physical Chemistry and The Fritz Haber Research Center, The Hebrew University, Jerusalem 91904, Israel

Thorsten Klüner[b]
Carl von Ossietzky Universität Oldenburg, Theoretische Physikalische Chemie, D-26111 Oldenburg, Germany

(Received 1 August 2005; accepted 1 November 2005; published online 9 January 2006)

The photodesorption of NO from NiO(100) is studied from first principles, with electronic relaxation treated by the use of the surrogate Hamiltonian approach. Two nuclear degrees of freedom of the adsorbate-substrate system are taken into account. To perform the quantum dynamical wave-packet calculations, a massively parallel implementation with a one-dimensional data decomposition had to be introduced. The calculated desorption probabilities and velocity distributions are in qualitative agreement with experimental data. The results are compared to those of stochastic wave-packet calculations where a sufficiently large number of quantum trajectories is propagated within a jumping wave-packet scenario. © *2006 American Institute of Physics*.
[DOI: 10.1063/1.2140697]

INTRODUCTION

Photochemistry of molecules adsorbed on surfaces continues to be a very active area of research.[1–4] While a vast amount of experimental data is available on this subject, the interpretation of experiments often requires a sophisticated theoretical analysis.[5–11] Even the simplest surface photochemical reaction, i.e., laser-induced desorption of a diatomic molecule from a surface, poses several challenges to theory. First of all, the calculation of reliable potential-energy surfaces (PESs) for the electronic states involved is an extremely difficult task although significant progress has been reported recently.[12,13] In general, these PESs are used as a prerequisite for subsequent simulations of the dynamics of nuclear motion which can be performed within the framework of quantum mechanics[14] or within (semi-) classical approaches.[15] The laser light induces an electronic excitation which is eventually quenched. This can be modeled on various levels of sophistication. In the spirit of a MGR (Menzel-Gomer-Redhead)[16,17] or Antoniewicz[18] scenario, electronic excitation and relaxation are treated as vertical transitions. Along these lines, Gadzuk proposed a stochastic wave-packet scheme where each wave packet spends a certain residence time on the electronically excited state. Observable properties of the desorbing molecules are then calculated by an incoherent average over a sufficiently large number of quantum trajectories. It was shown by Saalfrank that this jumping wave-packet approach is essentially equivalent to a solution of the Liouville-von Neumann equation for open systems, if the quenching rate is coordinate independent, i.e., the population of the electronically excited state decays exponentially.[19] In all of the above-mentioned schemes, empirical parameters need to be introduced. An alternative approach to the dissipative quantum dynamics of photodesorption was therefore pursued recently by Koch *et al.*[20,21] The system NO/NiO(100) was chosen in these studies for which detailed experimental data such as quantum state resolved velocity distributions have been obtained.[3] All steps of the photodesorption event were treated from first principles by a surrogate Hamiltonian approach.[22] However, the simulations were restricted to one dimension only, the desorption coordinate.

In the present paper, we extend this approach to two nuclear degrees of freedom for the first time. This necessitates the development of a parallelization strategy in order to use massively parallel computing resources. Our results will be systematically compared to stochastic wave-packet calculations for the same system. This allows us to investigate the extent to which the explicit treatment of electronic relaxation influences the results of experimentally observable quantities. In this sense, we provide a crucial check on the validity of semi-empirical approaches such as Gadzuk's jumping wave-packet approach in laser-induced desorption.

THEORY

To model the excitation-quenching cycle of photodesorption, we split the total system into primary system and

[a]Present address: Carl von Ossietzky Universität Oldenburg, Theoretische Physikalische Chemie, D-26111 Oldenburg, Germany.
[b]Author to whom correspondence should be addressed. Electronic mail: thorsten.kluener@uni-oldenburg.de

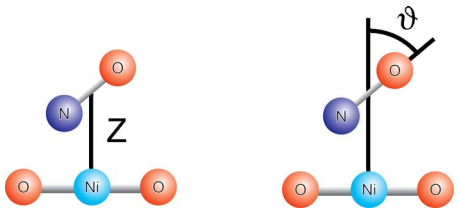

FIG. 1. The two nuclear degrees of freedom of the adsorbed molecule: the distance of the molecule to the surface Z and the polar angle ϑ between the molecular axis and the surface normal.

secondary bath parts. The primary system ($\hat{\mathbf{H}}_S$) corresponds to the adsorbed NO molecule on a finite part of the NiO surface while electron-hole pairs in the surface are modeled as environment or bath ($\hat{\mathbf{H}}_B$). Taking furthermore the interaction of the primary system with a driving field into account ($\hat{\mathbf{H}}_{SF}$), the total Hamiltonian is written as

$$\hat{\mathbf{H}}_{\text{tot}} = \hat{\mathbf{H}}_S + \hat{\mathbf{H}}_{SF}(t) + \hat{\mathbf{H}}_B + \hat{\mathbf{H}}_{SB}, \tag{1}$$

where $\hat{\mathbf{H}}_{SB}$ denotes the coupling between system and bath.

In the present study, the dynamics of nuclear motion in the adsorbate-substrate system NO/NiO(100) is simulated in two nuclear dimensions and on two electronic states. The two nuclear degrees of freedom taken into account are the desorption coordinate Z and the polar angle ϑ (see Fig. 1).

Electronic excitation

We assume that the laser pulse excites the adsorbed NO molecule from the electronic ground state to an intermediate NO^--like charge-transfer state.[23] The Hamiltonian of the primary system $\hat{\mathbf{H}}_S$ and the system-field interaction Hamiltonian $\hat{\mathbf{H}}_{SF}(t)$ may then be written as

$$\hat{\mathbf{H}}_S + \hat{\mathbf{H}}_{SF}(t) = \begin{pmatrix} \hat{\mathbf{T}} + V_g(Z,\vartheta) & E(t)\hat{\boldsymbol{\mu}}_{\text{tr}}(\hat{\mathbf{Z}}) \\ E^*(t)\hat{\boldsymbol{\mu}}_{\text{tr}}(\hat{\mathbf{Z}}) & \hat{\mathbf{T}} + V_e(Z,\vartheta) \end{pmatrix}. \tag{2}$$

In Eq. (2), the system Hamiltonian $\hat{\mathbf{H}}_S$ consists of the two-dimensional kinetic-energy operator $\hat{\mathbf{T}}$ and the PESs $V_{g/e}$ corresponding to the two electronic states involved.

Both two-dimensional PESs were constructed by Klüner *et al.*[12,24] V_g is a semi-empirical ground-state potential, while V_e represents the excited-state *ab initio* potential which was obtained within a valence configuration-interaction (CI) framework. The potential energy surfaces are displayed in Fig. 2. Due to the topology of the PESs around the Franck-Condon point, the wave packet will be accelerated toward the surface and toward smaller polar angles after a Franck-Condon excitation to the excited state.

TABLE I. Parameters for the laser pulse.

E_0	τ_P	$\hbar\omega_L$
8.5×10^{-3} a.u.	5 fs	3.7 eV

The system interacts with the electric field of the laser pulse $E(t)$ via the transition dipole operator $\hat{\boldsymbol{\mu}}_{\text{tr}}(Z)$. The coordinate dependence of $\hat{\boldsymbol{\mu}}_{\text{tr}}$ is obtained from *ab initio* calculations of the oscillator strength,[12,24] where the variation of $\hat{\boldsymbol{\mu}}_{\text{tr}}$ with respect to the polar angle ϑ is neglected. The field $E(t)$ is treated semi-classically, and its spatial dependence is omitted. Its shape is assumed to be Gaussian, $E(t) = E_0 \exp(-[(t-t_{\max})^2]/2\sigma_P^2)\exp(i\omega_L t)$. The laser pulse is therefore characterized by its carrier frequency ω_L, peak amplitude E_0, and full width at half maximum (FWHM) τ_P. The latter is related to the Gaussian standard deviation σ_P by $\tau_P = 2\sigma_P\sqrt{2\ln 2}$. The pulse parameters used in the present study are summarized in Table I. In accordance with experiment,[25,26] the laser frequency ω_L is taken to be $\hbar\omega_L = 3.7$ eV. We assume a resonant excitation, i.e., $\hbar\omega_L$ matches the difference of V_e and V_g at the minimum of the ground-state PES. In this model [Eq. (2)], only direct optical excitation of the adsorbed molecule is considered, while indirect, substrate-mediated excitation has been neglected. This is motivated by experimental results, which revealed a dependence of the desorption yield on the polarization of the laser light while desorption velocities were not influenced.[27] The polarization dependence indicates the importance of optical selection rules and hence the symmetry of the states involved. A localized charge-transfer excitation of the system is therefore a reasonable assumption. It supports a direct optical excitation within the adsorbate-substrate complex although an indirect excitation cannot be ruled out.

Electronic relaxation

The lifetime of the intermediate charge-transfer state has been estimated as about 15–25 fs.[12] Since an interaction with phonons requires lifetimes at least on the picosecond to nanosecond time scale, this possible relaxation channel is neglected in the present study. The excitation energy of the adsorbate-substrate complex dissipates into the surface due to interaction with electron-hole pairs in the surface. We ap-

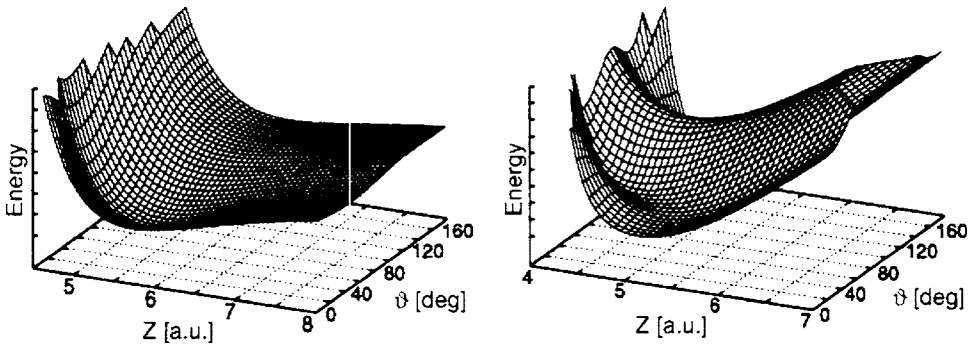

FIG. 2. Two-dimensional plots of the ground- (left) and excited-state PESs.

ply the surrogate Hamiltonian approach[20–22,28–30] to treat the electronic quenching of the excited-state population. In this method, the bath is approximated by a finite number of abstract, representative modes. In the limit of infinitely many bath modes, this "surrogate" bath Hamiltonian resembles the "true" bath Hamiltonian. However, in a finite time, the system can probe only a finite number N of bath modes, and $N \ll \infty$ is sufficient. By increasing the number N of bath modes, we can test the convergence of the method. We choose two level systems (TLSs) to describe our modes, i.e., a mode can be excited or deexcited. The Hilbert space of the bath $\mathcal{H}_B$ in the surrogate Hamiltonian approach has a dimension of 2^N. This corresponds to the number of all possible combinations of the two basis states of one TLS for N bath modes (i.e., none, one, two, … of the N TLSs excited at a time). It is possible to restrict the number of bath excitations which are allowed simultaneously in case not all of these combinations are necessary for a faithful representation of the bath.

In the present study, the TLSs model electron-hole pairs which are $O2p \rightarrow Ni3d$ charge-transfer states in the substrate. They are assumed to be localized on the sites of the NiO lattice. Delocalization is introduced by an interaction between neighboring TLSs. The Hamiltonian of this TLS bath is expressed as[20]

$$\hat{\mathbf{H}}_B = \varepsilon \sum_i \hat{\boldsymbol{\sigma}}_i^+ \hat{\boldsymbol{\sigma}}_i + \frac{\eta}{\log(N)} \sum_{ij(NN)} (\hat{\boldsymbol{\sigma}}_i^+ \hat{\boldsymbol{\sigma}}_j + \hat{\boldsymbol{\sigma}}_j^+ \hat{\boldsymbol{\sigma}}_i), \tag{3}$$

where $\hat{\boldsymbol{\sigma}}_i^+$ and $\hat{\boldsymbol{\sigma}}_i$ are creation and annihilation operators of the ith TLS, respectively. The first term describes excitation of a localized TLS at site i, while the second term takes the possibility of transport of excitation from one TLS to its nearest neighbors into account. The scaling factor $1/\log(N)$ results from the mapping of two dimensions of the bath onto one.[31]

Equation (3) introduces two parameters in the bath description, the excitation energy ε of the electron-hole pairs and the interaction strength η between nearest-neighbor TLSs. The latter leads to a finite width of excitation energy, i.e., an energy band of the bath. If the bath Hamiltonian, Eq. (3), is diagonalized, and N is the number of modes, N energies around ε corresponding to single excitations, N energies around 2ε corresponding to double excitations, etc., are obtained. The band structure of the bath is then characterized by these two parameters. The center of the energy band is fixed by ε, while its width is determined by η. The range of these parameters can be estimated by electron-energy-loss spectroscopy (EELS) as well as by CI calculations (see Ref. 20 and references therein). Due to the large band gap in NiO,[32–34] the energy of double excitations of bath modes is much higher than the laser energy of 3.7 eV. Hence, only the energy for a creation of one bath mode is in a suitable range to accept excitation energy from the system. Thus, it is justified to consider only single excitations, which reduces the dimension of $\mathcal{H}_B$ from 2^N to $N+1$. Consequently, the numerical effort is significantly decreased from exponential to linear scaling with respect to the number of bath modes. The description of the bath so far treats only electron-hole pairs in the uppermost layer of the NiO surface. However, vertical transport of excitation, i.e., transport into the surface, should also be accounted for. This is possible by considering several layers of bath modes. Each layer is treated as a separate bath into which dissipation of energy can take place, and neighboring layers are coupled analogously to Eq. (3). The coupling is determined by the interlayer coupling constant η_L.

The electron-hole pairs can be regarded as dipoles, and the laser excitation creates a nonzero transition dipole in the system. The system-bath interaction is therefore modeled as a dipole-dipole interaction between the system transition dipole $\hat{\vec{\boldsymbol{\mu}}}_S$ and the TLS of the bath,

$$\hat{\mathbf{H}}_{SB} = \begin{pmatrix} 0 & 1 \\ 1 & 0 \end{pmatrix} \otimes \sum_i \hat{\mathbf{V}}_i (\hat{\boldsymbol{\sigma}}_i^+ + \hat{\boldsymbol{\sigma}}_i). \tag{4}$$

The interaction potential $\hat{\mathbf{V}}_i$ is given by $\hat{\mathbf{V}}_i = \hat{\vec{\boldsymbol{\mu}}}_S \cdot \vec{\mathbf{E}}_i$, where $\vec{\mathbf{E}}_i$ is the electric field of the ith bath dipole. Note that $\hat{\mathbf{V}}_i$ is coordinate dependent since it depends on the distance between $\hat{\vec{\boldsymbol{\mu}}}_S$ and the ith bath dipole. Here, the bath dipoles parallel to the surface normal were incorporated into the simulation of electronic relaxation via dipole-dipole interaction (for details see Ref. 20).

Dynamics and observables

To simulate the complete photodesorption event within the microscopic model introduced above, a quantum dynamical wave-packet calculation is performed. In order to propagate the wave packet in time, the time evolution operator $\hat{\mathbf{U}}(t) = \exp(-i\hat{\mathbf{H}}t/\hbar)$ is expanded in Chebychev polynomials.[35] This results in a recursive application of the Hamiltonian to the wave function for each time step, where the kinetic-energy operator is applied in (angular) momentum space and the potential-energy operator in coordinate space, respectively.[35–38] Formally, the wave packet is represented by a five-dimensional array $\Psi(Z, \vartheta, \alpha, l, s)$. The nuclear dynamics of the primary system is simulated on a two-dimensional (Z, ϑ) grid. The index α labels the coordinate of the bath Hilbert space $\mathcal{H}_B$, while l denotes the (vertical) layer. The electronic degree of freedom s allows for a simultaneous propagation on the two PESs.

The propagation starts with the rovibrational ground state of the two-dimensional electronic ground-state potential with all bath modes deexcited. This corresponds to the absence of initial correlations between system and bath. This assumption is justified since no electron-hole pairs are thermally excited due to the large band gap of NiO of about 4 eV.[32–34] Note that, in principle, the surrogate Hamiltonian allows for taking initial correlations into account.[20]

The use of the surrogate Hamiltonian method allows for a simultaneous treatment of the charge-transfer dynamics as well as the electronic relaxation due to comparable time scales of both processes. The finite nature of the bath manifests itself as recurrences which appear in the simulation.

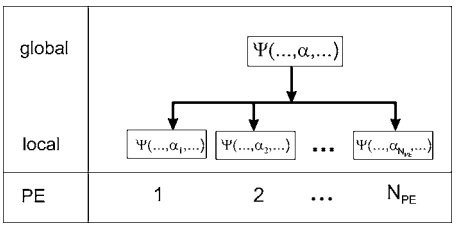

FIG. 3. Parallelization strategy: A one-dimensional data decomposition in the coordinate α is applied.

Energy transfer from the bath back to the system can be observed after a certain propagation time. At this recurrence time t_R, the system-bath coupling is switched off to avoid the excitation of the system by excited bath modes. In fact, excitation of the system via the surface does occur under certain experimental conditions such as high laser power and is known as a DIMET (desorption induced by multiple electronic transition) process. However, it was ruled out for the NO/NiO(100) experiments[27,39] for which a DIET (desorption induced by electronic transition) mechanism applies.

The recurrence time t_R can be prolonged by increasing the number of bath modes.[22] Thus, the use of a large number of modes N and of layers N_L significantly improves the convergence and allows for a longer propagation time. The electronic quenching happens on a much shorter time scale than the nuclear motion in the electronic ground state. Since the surrogate Hamiltonian approach is needed only for the description of electronic quenching, the propagation of the wave packet after t_R is continued without considering $\hat{\mathbf{H}}_B$ and $\hat{\mathbf{H}}_{SB}$ until converged observables in the asymptotic region ($V_g \approx 0$) of the electronic ground state are obtained. In order to obtain observables the wave packet is separated into a part in the interaction region ($V_g \neq 0$) and a part in the asymptotic region. The latter corresponds to desorbed molecules. The grid change procedure proposed by Heather and Metiu[40] is employed to transfer the wave packet onto an asymptotic grid. This allows for a simple propagation of a free particle in k-space.

Parallelization

To obtain converged observables in a reasonable computing time, a parallelization strategy had to be developed. The main objective of this strategy is to ensure a convenient data decomposition as well as load balancing between several processing elements (PEs). This means that each PE has to manage a similar amount of data and calculation effort. In the present study the above-mentioned array $\Psi(Z,\vartheta,\alpha,l,s)$ is decomposed in the coordinate α, i.e., the bath Hilbert space $\mathcal{H}_B$ is distributed to several PEs. This is illustrated in Fig. 3.

The advantage of such a parallelization strategy is the limited communication effort. Communication between different PEs is needed only for the application of $\hat{\mathbf{H}}_B$ and $\hat{\mathbf{H}}_{SB}$ to the wave function. The implementation is realized by message passing concepts of the Message Passing Interface (MPI) library.[41] Thus, the application of $\hat{\mathbf{H}}_{SB}$ to the wave packet within the Chebychev expansion could be implemented straightforwardly with global communication calls.[41]

TABLE II. Bath parameters (unless specified otherwise in the figure caption).

N	ε	η	N_L	η_L
31	37 eV	0.7 eV	15	0.3 eV

The Hamiltonian $\hat{\mathbf{H}}_B$ appears as a sparse band matrix in the bath Hilbert space $\mathcal{H}_B$ due to the nearest-neighbor interaction between the bath modes. The microscopic model of the bath implies the structure of $\hat{\mathbf{H}}_B$: the larger the dimension of the matrix is, the wider becomes the band of the matrix. Thus, the application of $\hat{\mathbf{H}}_B$ to the wave packet is equivalent to a matrix-vector multiplication, where each element of the vector represents a multidimensional array. A special scheme was developed to parallelize this matrix-vector multiplication, in which the matrix is decomposed line by line to several PEs. Then, the matrix-vector multiplication of the distributed data is processed locally and those parts of the array, which are needed from other PEs, are communicated. The structure of this communication scheme and the decomposition of the matrix could be processed before time evolution starts.

RESULTS

Comparison with 1D calculations

In the present section, we summarize the results of our two-dimensional surrogate Hamiltonian approach. The parameters of the laser pulse and the bath are in accordance with previous one-dimensional (1D) calculations,[20] and the most important values are summarized in Table II. First of all, we investigate the convergence properties of our approach. As mentioned in the previous section, the recurrence time t_R can be prolonged by increasing the number of bath modes. In the present description, the number of considered bath modes is equal to $N \cdot N_L$. Figure 4 shows the dependence of the population in the excited-state potential on propagation time. The prolongation of the recurrence time t_R with increasing number of layers N_L is clearly revealed.

This has also been demonstrated in previous 1D studies.[20] The role of the bath parameters with respect to the decay of excited-state population in those studies could be confirmed in the present two-dimensional calculations as shown in Fig. 4. As the bath parameters describe the electronic structure of the substrate which is independent of the dimensionality of nuclear dynamics, the results are indeed expected to be similar. Less population of bath modes in the interaction region, which is in the vicinity of the NO molecule, causes a decreasing interaction strength due to the structure of the system-bath interaction Hamiltonian [see Eq. (4)]. Therefore, an increasing value of η_L leads to a slower decay of excited-state population due to a faster transport of relaxed population out of the interaction region of the bath

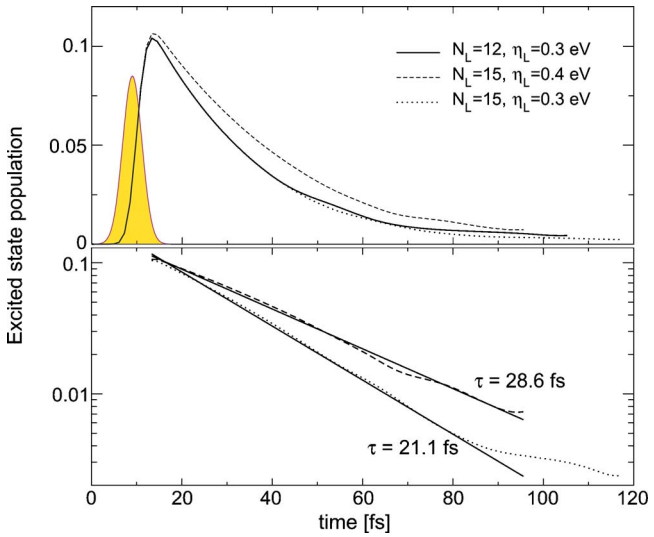

FIG. 4. Excited-state population vs time is shown on linear (top) and logarithmic (bottom) scales. The shape of the laser pulse is indicated in gray.

which implies a weaker system-bath interaction. After excitation by the laser pulse, an exponential decay of excited-state population can be observed, which allows for a determination of excited-state lifetime. The derived excited-state lifetime in Fig. 4 of about $\tau=21$ fs is in good agreement with the above-mentioned 1D calculations (25 fs)[21] and with previous simulations (25 fs).[42]

Despite the aforementioned similarities between 1D and 2D simulations, significant differences are observed as well. For instance, a longer propagation time is needed to get converged observables in the asymptotic region of the electronic ground state as shown in Fig. 5. While in the 1D calculations propagation times of about 3 ps were sufficient, we had to propagate our 2D wave packets for at least 14 ps to get a converged norm in the asymptotic region n_{asy}. This can be rationalized by the enlargement of configuration space with the extension to two dimensions, which causes longer path lengths of the molecules until the desorption event is completed. Increasing the number of layers (N_L) results in a longer recurrence time, while a stronger interlayer coupling (η_L) prolongs the excited-state lifetime (Fig. 4). Both effects

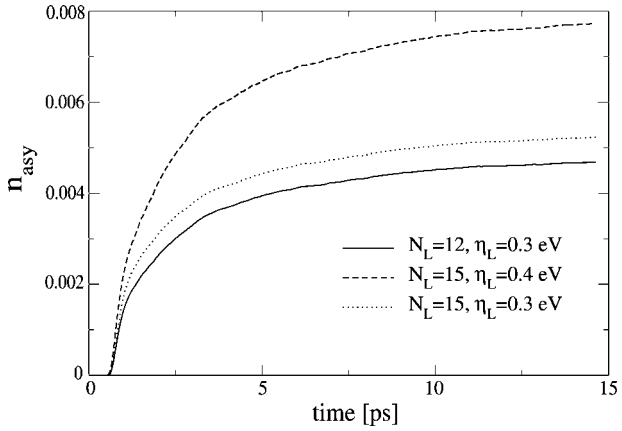

FIG. 5. Dependence of the norm of the wave packet in the asymptotic region n_{asy} on propagation time, number of bath layers, and interlayer interaction strength.

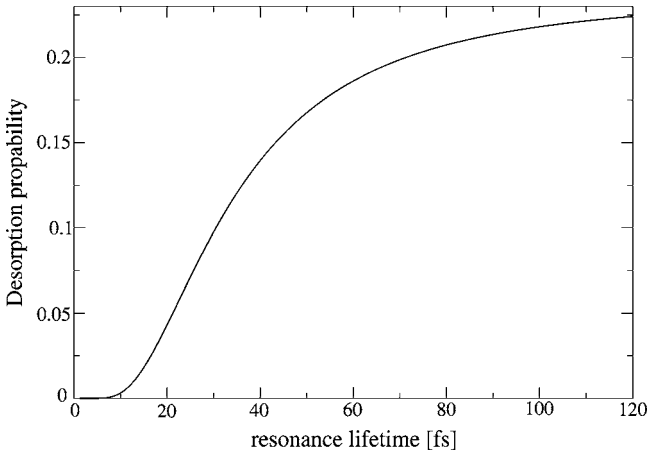

FIG. 6. Dependence of the desorption probability on the chosen resonance lifetime τ after averaging in the stochastic wave-packet calculation.

enhance desorption (Fig. 5), although a different microscopic meaning is associated. While η_L describes a property of the electronic structure of the substrate, the number of layers can simply be regarded as a technical parameter of the microscopic bath model within the surrogate Hamiltonian approach. Thus, η_L is a true physical parameter, while N_L should be increased until asymptotic observables are unaffected by the actual value of N_L. As one observable of interest, we calculate the desorption probability per excitation event P_{des}, which could be estimated from experimental desorption cross sections. P_{des} is obtained by normalizing n_{asy} with the excitation probability. Furthermore, the amount of excited-state population, which is neglected after switching off the bath, is added to the asymptotic norm n_{asy} before normalization to get an upper bound to the value of P_{des}.[20] Depending on the choice of the parameters, we calculated desorption probabilities P_{des} between 6.5% and 9%, which is in reasonable agreement with estimates from experiment.[43–45]

Comparison with stochastic wave-packet calculations

The calculations within the surrogate Hamiltonian approach were compared to stochastic wave-packet calcula-

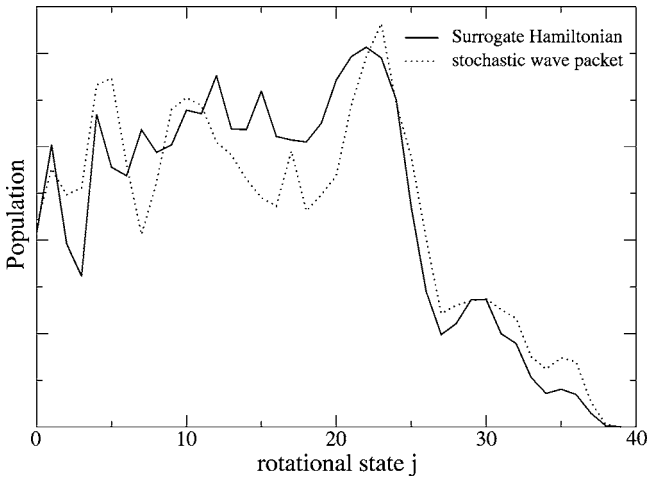

FIG. 7. Population of rotational states j of the desorbing molecules for stochastic wave-packet and surrogate Hamiltonian approaches.

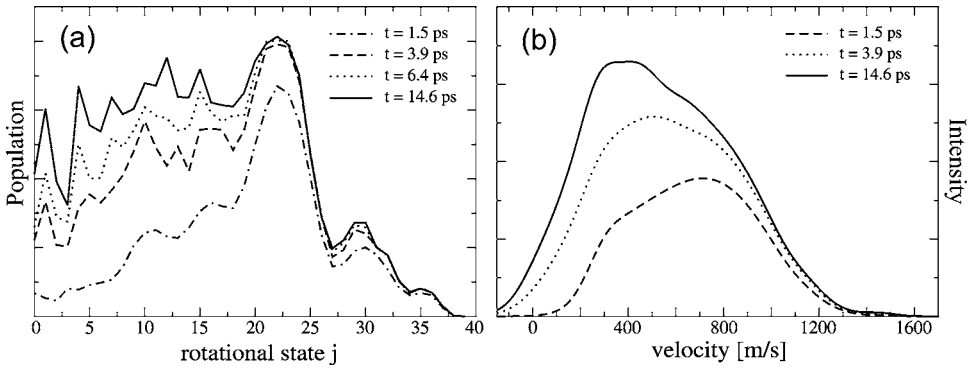

FIG. 8. Population of the rotational states j (left) and total velocity distributions of the desorbing molecules (right) for different propagation times. The fast molecules in high rotational states desorb first.

tions according to Gadzuk, where an incoherent averaging scheme over N_{tra} quantum trajectories is applied.[46] In this scheme, the laser excitation is modeled as a Franck-Condon excitation of the rovibrational ground-state PES to the excited-state PES. After a certain residence lifetime τ_n the wave packet is transferred back to the electronic ground-state PES and propagated up to convergence of observables in the asymptotic region. The expectation value of an observable $\hat{\mathbf{O}}$ is obtained from the asymptotic wave functions $\Psi_A(\tau_n)$ according to

$$\langle \hat{\mathbf{O}} \rangle(\tau) = \frac{\sum_{n=1}^{N_{\mathrm{tra}}} \exp(-\tau_n/\tau)\langle \Psi_A(\tau_n)|\hat{\mathbf{O}}|\Psi_A(\tau_n)\rangle}{\sum_{n=1}^{N_{\mathrm{tra}}} \exp(-\tau_n/\tau)\langle \Psi_A(\tau_n)|\Psi_A(\tau_n)\rangle}. \tag{5}$$

The averaging over N_{tra} single quantum trajectories with the exponential factor $\exp(-\tau_n/\tau)$ was introduced to model a dissipative scenario. The resonance lifetime τ is an empirical parameter in this method. This can be regarded as a drawback compared to the *ab initio* nature of the surrogate Hamiltonian approach, where the excited-state lifetime can be obtained from the decay rate of excited-state population. Furthermore, another essential distinction with respect to the decay of excited-state population between the two approaches should be mentioned. The averaging scheme simulates a coordinate-independent decay, while in the surrogate Hamiltonian approach, the decay is caused by dipole-dipole interaction between system and bath which shows a pronounced coordinate dependence.

In the stochastic wave-packet calculations $N_{\mathrm{tra}}=50$ quantum trajectories were propagated with residence lifetimes $\tau_R=5-242$ fs. A resonance lifetime of $\tau=24.2$ fs was chosen according to the excited-state lifetime deduced from the decay rate of excited-state population within our surrogate Hamiltonian approach (see Fig. 4). Using this resonance lifetime, we determine a desorption probability of $P_{\mathrm{des}} \approx 6.7\%$ (Fig. 6), which is compatible with the desorption probability of surrogate Hamiltonian calculations and with estimates from experiment.[43–45]

In addition to desorption probability, we compared the population of rotational states performing surrogate Hamiltonian and stochastic wave-packet calculations. Comparative results are summarized in Fig. 7, where the similarities of both approaches are revealed. The high rotational excitation can be rationalized by analyzing the topology of the excited-state PES. The wave packet is rotationally accelerated in the excited-state PES, while the gradient of the polar angle ϑ in the electronic ground-state potential is much less pronounced.

To get further insight into the dynamics of the wave-packet propagation with a surrogate Hamiltonian, it is useful to monitor the time evolution of some observables of the desorbing wave packet. The change of the rotational state population with an increasing propagation time is presented in Fig. 8(a). Obviously, the molecules in the higher rotational states desorb first. In principle, all desorbing molecules in rotational states $j \geqslant 23$ desorb already after a propagation time of $t=3.9$ ps. The molecules in the lower rotational states exhibit an opposite behavior since a late desorption occurs.

The total velocity distributions in Fig. 8(b) reveal a similar behavior with respect to time evolution. Experimentally, a bimodality of velocity distributions and a coupling of translation and rotation for the fast channel of the desorbing molecules are observed, i.e., rotationally excited molecules usually exhibit higher desorption velocities as well.[3] In order to elucidate this experimental feature, the velocity distributions for different rotational states j are plotted in Fig. 9.

The calculated velocity range is smaller as compared to experiment, where velocities up to 2000 m/s were measured. The bimodality is visible, especially for lower rotational states. The coupling of rotation and translation is observed not only for molecules with high velocities but also for slowly desorbing species. In fact, this discrepancy between experimental results and our theoretical simulations could be due to several reasons: First of all, the restricted dimension-

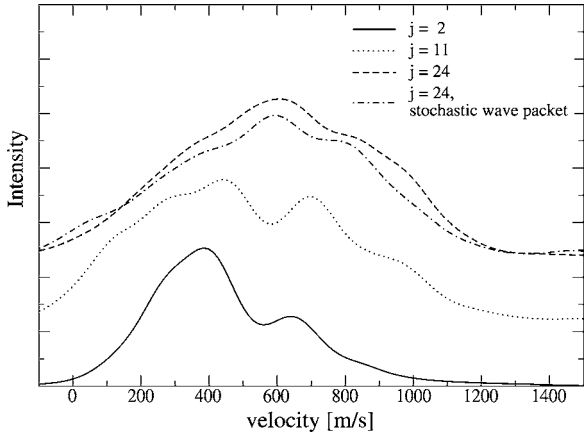

FIG. 9. Velocity distributions for different rotational states j. The bimodality and the coupling to the rotational states are visible.

ality of our studies should be mentioned. While a 2D treatment of nuclear motion can reproduce the main experimental features of the NO/NiO system, often multidimensional calculations have to be performed.[10,13,47,48] Furthermore, the results significantly depend on topological details of the PES, which might change upon further improvements of electronic structure calculations for ground and excited states of the NO/NiO system.[13] Nevertheless, important consequences are revealed by the present study. The similarity of the results obtained by stochastic wave-packet calculations and our surrogate Hamiltonian approach is evident. In both strategies, bimodal velocity distributions, similar desorption probabilities, and comparative rotational state populations could be obtained. As an illustrating example, velocity distributions for various rotational states and both approaches are summarized in Fig. 9. Here, the similarities of the velocity distributions of the two dissipative approaches are pointed out for $j=24$. Clearly, specific characteristics of the excitation process as well as the details of electronic relaxation do not severely affect experimental observables.

CONCLUSIONS

In the present study, laser-induced desorption of NO from NiO(100) was investigated from first principles within a surrogate Hamiltonian approach. Our current implementation is based on an extension of a one-dimensional treatment of laser-induced desorption proposed by Koch *et al.*[20,31] A direct optical excitation of the adsorbate-substrate system is modeled by an electronic transition from the ground state to a representative charge-transfer state. The simulation of the subsequent relaxation of the molecule is based on a simplified model of electronic quenching as a dipole-dipole interaction between the system transition dipole and electron-hole pairs in the surface. Since a massively parallel implementation could be realized, a two-dimensional simulation of the nuclear dynamics with a surrogate Hamiltonian becomes feasible for the first time.

The main advantage of this approach, as demonstrated previously, represents a consistent treatment of all steps of laser-induced desorption from first principles. However, a multidimensional treatment of nuclear motion necessitates an efficient massively parallel implementation of the surrogate Hamiltonian scheme.

In the present two-dimensional study, the main experimental features are reproduced: First of all, the calculated desorption probability is similar to estimates from experiment, and secondly the state resolved velocity distributions exhibit the experimentally observed bimodality as well as a correlation between translational and rotational motion of the desorbing molecules. In accordance with a previous study,[13] the bimodality of velocity distributions could be traced back to the topology of the potential energy surfaces involved. The value of the present study manifests itself in the invariance of the general physics underlying laser-induced desorption with respect to the explicit treatment of electronic relaxation. In fact, both approaches investigated in the present study yielded qualitatively identical results. Therefore, our results suggest that a faithful description of laser-induced desorption experiments depend strongly on reliable PES but could be insensitive with respect to details of explicit models of nuclear dynamics chosen in a particular study.

ACKNOWLEDGMENTS

We thank S. Borowski for many fruitful discussions. Computer resources provided by the Rechenzentrum der Max-Planck-Gesellschaft Garching are gratefully acknowledged.

[1] S. Kwiet, D. E. Starr, A. Grujic, M. Wolf, and A. Hotzel, Appl. Phys. B: Lasers Opt. **80**, 115 (2004).
[2] T. G. Lee and J. C. Polanyi, Surf. Sci. **462**, 36 (2000).
[3] T. Mull, B. Baumeister, M. Menges, H.-J. Freund, D. Weide, C. Fischer, and P. Andresen, J. Chem. Phys. **96**, 7108 (1992).
[4] B. Redlich, L. van der Meer, H. Zacharias, G. Meijer, and G. von Helden, Nucl. Instrum. Methods Phys. Res. A **507**, 556 (2003).
[5] E. Hasselbrink, M. Wolf, S. Holloway, and P. Saalfrank, Surf. Sci. **363**, 179 (1996).
[6] H. Guo and G. Ma, J. Chem. Phys. **111**, 8595 (1999).
[7] A. Abe and K. Yamashita, J. Chem. Phys. **119**, 9710 (2003).
[8] M. Nest and P. Saalfrank, J. Chem. Phys. **116**, 7189 (2002).
[9] M. Nest and P. Saalfrank, Phys. Rev. B **69**, 235405 (2004).
[10] S. Borowski, T. Klüner, and H.-J. Freund, J. Chem. Phys. **119**, 10367 (2003).
[11] M. P. de Lara-Castells and J. L. Krause, J. Chem. Phys. **118**, 5098 (2003).
[12] T. Klüner, H.-J. Freund, J. Freitag, and V. Staemmler, J. Chem. Phys. **104**, 10030 (1996).
[13] D. Kröner, I. Mehdaoui, H.-J. Freund, and T. Klüner, Chem. Phys. Lett. **415**, 150 (2005).
[14] H. Guo, P. Saalfrank, and T. Seidemann, Prog. Surf. Sci. **62**, 239 (1999).
[15] J. C. Tully, J. Chem. Phys. **93**, 1061 (1990).
[16] D. Menzel and R. Gomer, J. Chem. Phys. **41**, 3311 (1964).
[17] P. A. Redhead, J. Chem. Phys. **41**, 886 (1964).
[18] P. R. Antoniewicz, Phys. Rev. B **21**, 3811 (1980).
[19] P. Saalfrank, Chem. Phys. **211**, 265 (1996).
[20] C. P. Koch, T. Klüner, H.-J. Freund, and R. Kosloff, J. Chem. Phys. **119**, 1750 (2003).
[21] C. P. Koch, T. Klüner, H.-J. Freund, and R. Kosloff, Phys. Rev. Lett. **90**, 117601 (2003).
[22] R. Baer and R. Kosloff, J. Chem. Phys. **106**, 8892 (1997).
[23] T. Klüner, S. Thiel, H.-J. Freund, and V. Staemmler, Chem. Phys. Lett. **294**, 413 (1998).
[24] T. Klüner, Ph.D. thesis, Ruhr-Universität Bochum, 1997.
[25] C. Rakete, Ph.D. thesis, Freie Universität Berlin, 2004.
[26] A. Braun, Diploma thesis, Freie Universität Berlin, 1999.
[27] H. Zacharias, G. Eichhorn, R. Schliesing, and K. Al-Shamery, Appl. Phys. B: Lasers Opt. **68**, 605 (1999).
[28] C. P. Koch, T. Klüner, and R. Kosloff, J. Chem. Phys. **116**, 7983 (2002).
[29] D. Gelman and R. Kosloff, Chem. Phys. Lett. **381**, 129 (2003).
[30] D. Gelman, C. P. Koch, and R. Kosloff, J. Chem. Phys. **121**, 661 (2004).
[31] C. P. Koch, Ph.D. thesis, Humboldt-Universität Berlin, 2002, http://edoc.hu-berlin.de/docviews/abstract.php?lang=ger&lang=ger&id=10526
[32] H.-J. Freund, Faraday Discuss. **114**, 1 (1999).
[33] G. J. M. Jansen and W. C. Nieuwpoort, Phys. Rev. B **38**, 3449 (1988).
[34] F. Aryasetiawan and O. Gunnarson, Phys. Rev. Lett. **74**, 3221 (1995).
[35] R. Kosloff, J. Phys. Chem. **92**, 2087 (1988).
[36] R. Kosloff, Annu. Rev. Phys. Chem. **45**, 145 (1994).
[37] G. C. Corey and D. Lemoine, J. Chem. Phys. **97**, 4115 (1992).
[38] G. C. Corey and J. Tromp, J. Chem. Phys. **103**, 1812 (1995).
[39] G. Eichhorn, M. Richter, K. Al-Shamery, and H. Zacharias, J. Chem. Phys. **111**, 386 (1999).
[40] R. Heather and H. Metiu, J. Chem. Phys. **86**, 5009 (1987).
[41] Message Passing Interface Forum, MPI: A Message-Passing Interface Standard, Knoxville, Tennessee (1995), University of Tennessee.
[42] T. Klüner, H.-J. Freund, V. Staemmler, and R. Kosloff, Phys. Rev. Lett. **80**, 5208 (1998).
[43] M. Menges, B. Baumeister, K. Al-Shamery, H.-J. Freund, C. Fischer, and P. Andresen, J. Chem. Phys. **101**, 3318 (1994).

[44] P. Saalfrank, Chem. Phys. **193**, 119 (1995).
[45] J. W. Gadzuk, L. J. Richter, S. A. Buntin, D. S. King, and R. R. Cavanagh, Surf. Sci. **235**, 317 (1990).
[46] J. W. Gadzuk, Surf. Sci. **342**, 345 (1995).
[47] S. Borowski, T. Klüner, H.-J. Freund, I. Klinkmann, K. Al-Shamery, M. Pykavy, and V. Staemmler, Appl. Phys. A: Mater. Sci. Process. **78**, 223 (2004).
[48] C. Bach, T. Klüner, and A. Groß, Chem. Phys. Lett. **376**, 424 (2003).